

Wintertime CO₂ fluxes in an Arctic polynya using eddy covariance: Evidence for enhanced air-sea gas transfer during ice formation

B. G. T. Else,¹ T. N. Papakyriakou,¹ R. J. Galley,¹ W. M. Drennan,² L. A. Miller,³ and H. Thomas⁴

Received 27 October 2010; revised 19 April 2011; accepted 14 June 2011; published 20 September 2011.

[1] Between Nov. 1 2007 and Jan. 31 2008, we calculated the air-sea flux of CO₂, sensible heat, and water vapor in an Arctic polynya system (Amundsen Gulf, Canada) using eddy covariance equipment deployed on the research icebreaker *CCGS Amundsen*. During this time period, Amundsen Gulf was a dynamic sea ice environment composed primarily of first year ice with open water coverage varying between 1–14%. In all cases where measurements were influenced by open water we measured CO₂ fluxes that were 1–2 orders of magnitude higher than those expected under similar conditions in the open ocean. Fluxes were typically directed toward the water surface with a mean flux of $-4.88 \mu\text{mol m}^{-2} \text{s}^{-1}$ and a maximum of $-27.95 \mu\text{mol m}^{-2} \text{s}^{-1}$. One case of rapid outgassing (mean value $+2.10 \mu\text{mol m}^{-2} \text{s}^{-1}$) was also observed. The consistent pattern of enhanced gas exchange over open water allows us to hypothesize that high water-side turbulence is the main cause of these events. Modification of the physical and chemical properties of the surface seawater by cooling and brine rejection may also play a role. A rough calculation using an estimate of open water coverage suggests that the contribution of these events to the annual regional air-sea CO₂ exchange budget may make the winter months as important as the open water months. Although high, the uptake of CO₂ fits within mixed layer dissolved inorganic carbon budgets derived for the region by other investigators.

Citation: Else, B. G. T., T. N. Papakyriakou, R. J. Galley, W. M. Drennan, L. A. Miller, and H. Thomas (2011), Wintertime CO₂ fluxes in an Arctic polynya using eddy covariance: Evidence for enhanced air-sea gas transfer during ice formation, *J. Geophys. Res.*, 116, C00G03, doi:10.1029/2010JC006760.

1. Introduction

[2] In order to properly forecast the effects of climate change, general circulation models need to adequately account for sources and sinks of CO₂. The global marine system plays a major role in cycling CO₂ and presently absorbs about 2.2 PgC year⁻¹ [Denman *et al.*, 2007], which offsets about 30% of present anthropogenic emissions. However, the rate of CO₂ uptake is not consistent across all oceans. On an annual basis a given region may behave anywhere on the spectrum from a strong source of CO₂ to a strong sink, and significant inter- and intra-annual variability may also exist [Takahashi *et al.*, 2009]. This spatiotemporal

variability arises from variability in the processes controlling CO₂ fluxes.

[3] For the open ocean, research has advanced to the point where these processes are known well enough to make reasonable flux estimates at a wide range of scales (see review by Wanninkhof *et al.* [2009]). Typically, estimates of CO₂ flux (F_{CO_2}) are computed using a form of the bulk flux equation:

$$F_{\text{CO}_2} = \alpha k (p\text{CO}_{2\text{sw}} - p\text{CO}_{2\text{air}}) \quad (1)$$

where α is the solubility of CO₂ in water, $p\text{CO}_{2\text{sw}}$ is the partial pressure of CO₂ in the surface seawater, $p\text{CO}_{2\text{air}}$ is the partial pressure of CO₂ in the atmosphere and k is the gas transfer velocity. Using this approach, the air-sea gradient of CO₂ ($p\text{CO}_{2\text{sw}} - p\text{CO}_{2\text{air}}$, commonly denoted $\Delta p\text{CO}_2$) determines the potential for exchange, while the transfer velocity encompasses the processes that control the rate at which the exchange can occur. The main determinant of transfer velocity is water-side turbulence, which itself is mainly determined by wind velocity through its relationship with momentum flux [Jähne, 1987]. Many other factors influence water-side turbulence, such as wave state [Bock *et al.*, 1999; Zappa *et al.*, 2004], surface films [Jähne, 1987;

¹Centre for Earth Observation Science, Department of Environment and Geography, University of Manitoba, Winnipeg, Manitoba, Canada.

²Division of Applied Marine Physics, Rosenstiel School of Marine and Atmospheric Science, University of Miami, Miami, Florida, USA.

³Centre for Ocean Climate Chemistry, Institute of Ocean Sciences, Fisheries and Oceans Canada, Sidney, British Columbia, Canada.

⁴Department of Oceanography, Dalhousie University, Halifax, Nova Scotia, Canada.

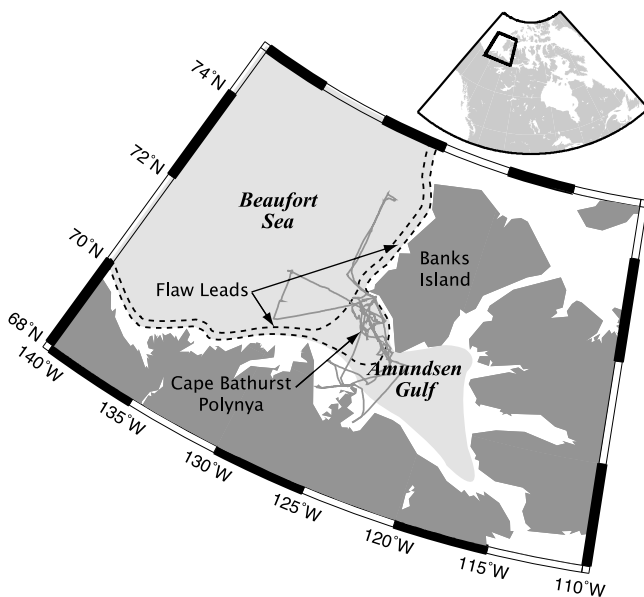


Figure 1. Map of the Banks Island flaw lead/polynya complex. The light grey line shows the ship track. The shaded grey area represents the region which usually remains mobile through the time period under consideration, and the dotted line shows the areas typically associated with the Cape Bathurst polynya and flaw lead.

Frew *et al.*, 2004; Frew, 1997], rain [Ho *et al.*, 2004; Takagaki and Komori, 2007; Zappa *et al.*, 2009], tides [Zappa *et al.*, 2007], and buoyancy [McGillis *et al.*, 2004]. In addition, several processes not directly related to turbulence also affect transfer velocity, such as chemical enhancement [Bolin, 1960; Kuss and Schneider, 2004] and bubbles from breaking waves [Asher *et al.*, 1996; Woolf, 1997; Woolf *et al.*, 2007]. Despite the myriad processes affecting gas exchange, wind velocity alone is typically used to estimate transfer velocity in the open ocean with mature wavefields [Wanninkhof *et al.*, 2009]. As such, numerous parameterizations to estimate k from wind speed have been created based on tank experiments [Liss and Merlivat, 1986], modeling exercises [Wanninkhof, 1992; Sweeney *et al.*, 2007], and field studies conducted primarily at low and midlatitudes [Ho *et al.*, 2006; Nightingale *et al.*, 2000; Wanninkhof and McGillis, 1999].

[4] At high latitudes (e.g. the Arctic), the processes that control CO₂ fluxes are not well known. Depending on the season and location, a given region of the Arctic Ocean may be ice free or it may be covered by sea ice of variable concentration, thickness and thermodynamic state. During the open water season it is reasonable to assume that what we understand about open-ocean fluxes would be applicable, but as soon as sea ice is present existing parameterizations of transfer velocity are likely invalid. Although sea ice is permeable to gas exchange under certain conditions [Gosink *et al.*, 1976], the mechanisms that control the rate of exchange are very different from the open ocean. Furthermore, the open water that does remain in an icescape experiences different controls on near-surface turbulence; fetch limitations [Woolf, 2005] imposed by surrounding ice floes and the generation of turbulence due to ice formation

[McPhee and Stanton, 1996] are two examples of those unique controls.

[5] The initial freezeup and growth of sea ice has generated considerable interest, since the process significantly modifies the chemistry of the surface ocean and because dissolved inorganic carbon (DIC) may be driven down from the surface with rejected brines in what has been termed a sea ice CO₂ pump [Rysgaard *et al.*, 2007, 2009; Anderson *et al.*, 2004]. A water column study by Anderson *et al.* [2004] in Svalbard found high DIC and elevated chlorofluorocarbon levels in deep waters, which they hypothesized originated from enhanced air-sea exchange of CO₂ during ice formation. Some support for this enhanced exchange was recently presented in a tank study by Loose *et al.* [2009]. In this paper, we describe the first eddy covariance observations of such flux enhancements over a natural sea ice surface.

2. Study Area

[6] The data presented in this paper were collected between Nov. 1, 2007 and Jan. 31, 2008 during the International Polar Year Circumpolar Flaw Lead System Study (CFL) in Amundsen Gulf and the southeaster Beaufort Sea (Figure 1). The region is subject to a complex annual ice cycle which has been summarized by Galley *et al.* [2008]. The open water season (defined as sea ice concentration $\leq 20\%$) typically lasts 10 weeks, starting in late July. Freezeup occurs in early October and is characterized by initial landfast ice growth along the coastal margins. The ice which forms offshore in Amundsen Gulf typically remains mobile during the time period of this study (shaded areas in Figure 1), creating an icescape which is characterized by small transient leads and polynyas. Later in the winter the eastern half of Amundsen Gulf may become landfast, and on some occasions the western portion becomes landfast as well. The Beaufort Sea pack ice remains mobile throughout the winter, rotating with the predominant Beaufort gyre to create persistent linear flaw lead features (Figure 1). The mean spring breakup for Amundsen Gulf is early June, which creates the feature commonly referred to as the Cape Bathurst polynya (Figure 1) which in some years extends well into eastern Amundsen Gulf.

[7] Observations have shown that the region experiences significant air-sea $p\text{CO}_2$ gradients in the fall. Mucci *et al.* [2010] observed $\Delta p\text{CO}_2$ ranging from -138 to -28 μatm from Sep.–Nov. 2003, and Murata and Takizawa [2003] observed gradients of similar magnitude during three years of cruises in Aug.–Sep., 1998–2000. Observations made during the CFL study showed that significant undersaturation ($\Delta p\text{CO}_2$ typically around -70 μatm) persisted through the end of January 2008 in offshore Amundsen Gulf [Shadwick *et al.*, 2011].

[8] During the winter season, the persistent flaw leads and polynyas in combination with strong local $p\text{CO}_2$ gradients make this study area an ideal location for examining the effect of freezing sea ice on gas exchange.

3. Methods

3.1. Atmospheric Instrumentation

[9] For the duration of the experiment a guyed open-lattice tower at the bow of the ship was instrumented with

eddy covariance and meteorological equipment. The flux instrumentation consisted of a Gill Windmaster Pro sonic anemometer/thermometer, a LI-COR LI-7500 open path CO₂/H₂O gas analyzer and a Systron Donner MotionPak. The flux instrumentation was located at a height of 14 m above the surface (7 m above the deck of the ship), with the exception of the MotionPak which was located at the mid-point of the tower.

[10] The meteorological equipment consisted of a conventional anemometer for wind speed and direction (RM Young 05103, height = 15 m), a temperature/relative humidity probe (Vaisala HMP45C212, height = 14 m) and a pressure sensor (RM Young 61205V). An array of radiation sensors was deployed on top of the wheelhouse of the ship, consisting of a photosynthetically active radiation (PAR) sensor (Kipp and Zonen PARlite), an incoming shortwave radiation sensor (Eppley PSP) and an incoming longwave radiation sensor (Eppley PIR).

3.2. Surface Water pCO₂ Instrumentation

[11] Surface water from a dedicated scientific intake line (depth ~5 m) was continuously sampled for pCO_{2sw} using a shower-type equilibrator which cycled headspace air through a LI-COR LI-7000 CO₂/H₂O gas analyzer [Körtzinger *et al.*, 1996]. The gas analyzer was calibrated daily using ultra-high purity N₂ as a zero gas and a CO₂/air mixture traceable to WMO standards as a span gas. The instrument was located in the engine room very close to the water intake, but a slight warming of the sample water relative to results from CTD casts was detected by a thermocouple in the equilibrator. This warming effect was very consistent, allowing correction of pCO_{2sw} for thermodynamic effects following Takahashi *et al.* [1993]. After correction, the pCO_{2sw} measurements showed good agreement (r² = 0.9, mean difference = 19 μatm, no statistically significant bias) with independent calculations from DIC/TA measurements (see Shadwick *et al.* [2011] for a description of the DIC/TA data set and methods).

3.3. Study Design

[12] The CFL study was a unique over-wintering experiment because the research vessel remained mobile through the entire winter. The goal of this strategy was to create a time series of the seasonal evolution of the flaw lead/polynta system. Logistically, this meant that the specific location and operation of the vessel was highly opportunistic; when ice conditions allowed ship to move freely, spatial sampling was conducted, but when ice conditions were more severe the ship was positioned in large consolidated floes and allowed to drift. These floes were typically occupied for 1–7 days, depending on the stability of the floe and whether or not it was drifting outside of the study area. When repositioning was necessary, the ship would break out of the floe and either break ice or transit through small flaw leads until a more suitable floe was located.

3.4. Eddy Covariance

[13] The study design allowed us to examine a sea ice system which would otherwise be inaccessible, but it does have implications for the eddy covariance technique which is best suited for a stationary tower over a homogenous

surface. To help address these issues, we filtered the data to ensure that each eddy covariance run was not subject to significant changes either in ship operation or atmospheric conditions. If the ship was under power, ship velocity and course over ground were required to be consistent (within ±3.7 km hr⁻¹ of mean for velocity and ±27.5° of mean for course). Relative wind direction was also required to be consistent within ±27.5° of the mean, and it was further restricted to within ±90° of the bow of the ship to reduce the effects of flow distortion. To help with the issue of non-homogeneous surfaces, we found it useful to break the data up into individual case studies during time periods where flux data collection was consistent and the ship location, atmospheric conditions and sea ice conditions were fairly uniform (see Table 1 and Figure 2).

[14] Filtering was also necessary to remove instances where atmospheric conditions negatively impacted the flux instruments. The LI-7500 outputs a diagnostic value that warns of lens obstruction, which during this study was most often caused by accretion of rime. We filtered out all instances where the diagnostic value exceeded its normal operating range, creating a fairly significant loss of data. The sonic anemometer was less influenced by riming, but filtering was carried out based on the characteristically erratic performance of the instrument that occurs under such circumstances.

[15] The LI-7500 used in this study makes high frequency (10Hz) measurements of the molar concentrations of CO₂ and water vapor (c_{CO_2} and c_v , respectively). By combining these measurements with high frequency vertical wind velocity (w) measurements from the sonic anemometer, the flux of CO₂ is calculated over an averaging period (in this case, 30 minutes) via:

$$F_c = \overline{w'c'_{CO_2}} + \frac{\overline{c_{CO_2}}}{\overline{c_d}} \left[\overline{w'c'_v} + \overline{c_a} \frac{\overline{w'T'}}{\overline{T}} \right] \quad (2)$$

where the overbars denote averaged quantities, the primes indicate fluctuations around a mean value, T is air temperature, c_d is the dry air molar concentration, and c_a is the moist air molar concentration [Leuning, 2004]. The second term on the right hand side of equation (2) is the so-called WPL correction (or dilution correction) that must be used for open path sensors [Webb *et al.*, 1980]. The necessary high frequency T measurements are determined from sonic temperature (measured by the sonic anemometer), which were converted to T following Kaimal and Gaynor [1991]. The MotionPak provides 3-axis measurements of acceleration and angular velocity which were used to correct w for ship motion. The techniques for this correction were first adapted for ships by Mitsuta and Fujitani [1974], and later refined by other investigators [Fujitani, 1981; Dugan *et al.*, 1991; Ancil *et al.*, 1994; Edson *et al.*, 1998].

[16] The utility of open path sensors for measuring CO₂ fluxes has recently been debated for conditions where low fluxes are expected [Burba *et al.*, 2008; Amiro, 2010; Ono *et al.*, 2008] and in the marine environment [Prytherch *et al.*, 2010]. During the non-growing season over several terrestrial ecosystems, significant uptakes of CO₂ have been observed and identified as artifacts of the LI-7500 gas

Table 1. Summary of Conditions Experienced During Each Sample Case

Case	Date	Location (Lat/Lon)	CO ₂ Flux ($\mu\text{mol m}^{-2} \text{s}^{-1}$)	ΔCO_2 (μatm)	H Flux (W m^{-2})	E Flux (W m^{-2})	Air T ($^{\circ}\text{C}$)	Wind Vel. (m s^{-1})	Wind Dir. (deg)	Sea Ice Conditions
1	11/02 04:30– 11/03 09:30	71.185 ^a – 129.096	–1.81	–80	43.3	4.1	–7.5	8.7	29	Newly forming grease ice
2	11/08 02:15– 11/09 00:50	69.498– 123.930	0.23	146.5	7.3	3.7	–18.9	5.5	131.1	Newly forming fast ice. Estimated thickness: 30–40 cm
3	11/20 01:30– 11/20 14:45	71.038– 123.297	2.1	–77.4	53.8	9.9	–15.2	12.5	98.4	Mobile ice with upwind leads, thickness: 37 cm
4	11/20 16:00– 11/20 18:30	71.071– 123.430	–9.58	–66.7	111.4	11.3	–14.2	11.8	110.8	Mobile ice with upwind leads, thickness: 37 cm
5	11/28 07:30– 11/29 02:00	70.419 ^a – 126.372	0.55	15.8	–2.3	0.8	–16	8	254.6	Consolidated mobile ice, thickness: 52cm
6	11/30 05:15– 11/30 23:30	71.053 ^a – 123.954	–0.03	–52.1	1.3	–1.1	–15.8	11.5	314.1	Consolidated, ridged ice floe
7	12/01 07:00– 12/01 12:30	71.590 ^a – 124.656	–26.88	N/A	33.4	–10.4	–16.6	7.3	3.4	Transit through active lead with open water and grease ice
8	12/01 13:45– 12/02 02:45	71.901– 125.441	0.31	–63.6	–2.9	0	–19.7	5.1	37.3	Land fast ice
9	12/02 05:30– 12/02 22:15	71.725– 125.597	0.35	–69.4	1.3	–0.3	–18.2	3.4	47.1	Consolidated ice floe, thickness: 35cm
10	12/04 21:00– 12/06 12:15	71.402 ^a – 124.875	–0.09	–86.7	15.8	2	–18	5.1	267.3	Consolidated ice floes, varying thicknesses: 25–45 cm
11	12/19 23:15– 12/22 18:15	71.915– 125.433	0.42	–49.8	–0.6	3.3	–22	4.6	108.8	Land fast ice
12	12/24 20:45– 12/25 17:15	71.262– 124.383	–0.14	–51	5.5	1.3	–20.7	5.9	123.2	Consolidated mobile ice, thickness: 30 cm
13	01/02 18:15– 01/06 03:30	71.306 ^a – 124.722	–0.5	–52	–7.9	5.3	–21.8	11.6	117.9	Thick consolidated ice floe, thickness: 105 cm
14	01/10 09:15– 01/11 18:45	71.653 ^a – 126.101	0.58	–78.3	2.9	1.2	–21.3	7	123.3	Consolidated mobile ice
15	01/13 16:00– 01/14 22:00	71.494 ^a – 124.638	0.34	–73.8	3.2	1	–25	8	62.4	Consolidated mobile ice
16	01/20 17:00– 01/21 04:30	71.579– 125.104	0.34	N/A	–2.9	2.8	–18.9	6.4	123.6	Consolidated mobile ice, thickness: 91 cm
17	01/24 08:00– 01/25 05:30	71.203– 125.184	–3.15	–38.4	16.4	5.6	–20.3	11.9	291.7	Consolidated mobile ice, upwind leads
18	01/25 18:00– 01/26 16:30	71.172– 125.014	–0.86	–8.6	9.4	2	–25.7	8.7	298.5	Consolidated mobile ice

^aShip was in transit, or drifting significantly: reported value is the midpoint of the sampling period.

analyzer [Amiro, 2010; Ono *et al.*, 2008; Hirata *et al.*, 2007]. Work by Burba *et al.* [2008] have shown that a heat flux generated by the electronics of the LI-7500 is likely the most significant contributor to this bias, especially at low air temperatures. Other suggestions include pressure fluctuations at high wind velocities that are not usually included in the WPL correction [Järvi *et al.*, 2009] and incomplete WPL corrections due to poor energy balance closure [Ono *et al.*, 2008]. The magnitude of these discrepancies are usually on the order of $1 \mu\text{mol m}^{-2} \text{s}^{-1}$, which in most terrestrial systems during the growing season is a small percentage of the total flux. However, typical magnitudes of CO₂ flux in the open ocean are less than $1 \mu\text{mol m}^{-2} \text{s}^{-1}$ [e.g., McGillis *et al.*, 2001].

[17] A further difficulty of working with an open path analyzer in a marine environment is an apparent sensitivity to contamination of the sensor lens by impurities (most likely salt particles) [Kohsiek, 2000; Prytherch *et al.*, 2010]. The contamination appears to cause a portion of water vapor fluctuations to be mis-recorded as fluctuations of CO₂ (an effect known as “crosstalk”), and can lead to CO₂ fluxes an order of magnitude higher than expected [Prytherch *et al.*, 2010].

[18] Corrections have been proposed for both the sensor heating and H₂O crosstalk issues. Burba *et al.* [2008] proposed several ways in which the heat flux of the LI-7500 can be estimated and added to the WPL correction. In this study, we have adopted their multivariate regression model for determining the sensor heat flux from air temperature, wind velocity and incoming longwave/shortwave radiation. Prytherch *et al.* [2010] proposed a correction for the H₂O crosstalk (termed the “PKT” correction) in which an iterative approach is used to remove unwanted correlation between the CO₂ and H₂O signals. This correction has also been adopted for this study, but as we discuss in section 5.1 we found it to be unreliable. Thus, all CO₂ flux values reported herein include only the Burba *et al.* [2008] correction along with the usual WPL corrections.

3.5. RADARSAT-1 Imagery

[19] To aid in the identification of ice conditions and to quantify the amount of open water within the study area over the period, fourteen (14) RADARSAT-1 ScanSAR narrow beam images acquired between Nov. 6 2007 and Jan. 28 2008 were classified. RADARSAT-1 ScanSAR narrow beam mode has a resolution of 50 m and a nominal

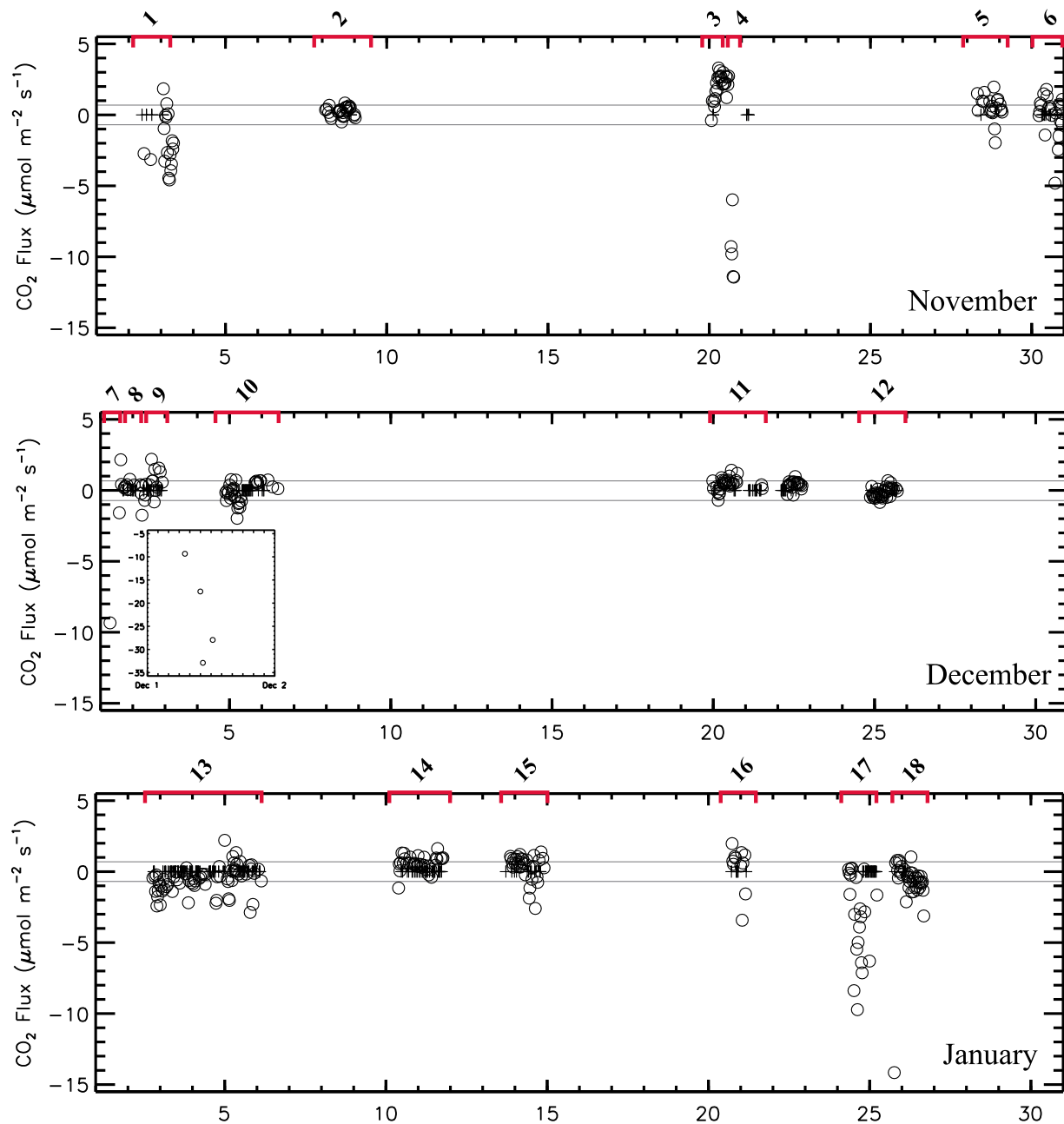


Figure 2. Measured CO₂ fluxes (including sensor heating correction) for the study period. The numbers along the top axis indicate the sample cases, the most interesting of which are discussed in the text, with the red brackets denoting their time frame. The inset shows observations made between Dec. 1–2 with an extended scale on the y-axis. The horizontal grey lines show the estimated noise level of the eddy covariance system as discussed in section 5.1.

coverage area of 300 x 300 km. Each of the images were geo-referenced and calibrated to σ^0 , then geographically cropped using latitudinal bounds 70° and 71.5°N and longitudinal bounds 122° and 126°W. The calibrated, geo-referenced sub-images were then subjected to a median filter with a 3 × 3 window size to reduce the “speckle” noise common to synthetic aperture RADAR (SAR) imagery while preserving edges. Edge preservation is very important when linear features such as leads are the predominant form of open water at this time of year. Finally, each sub-image was manually classified according to the principles set forth

by the Canadian Ice Service (CIS) SAR ice interpretation guide [Canadian Ice Service, 2002].

4. Results

4.1. Observations of High CO₂ Flux Events

4.1.1. Case 1: Nov. 2 04:30–Nov. 3 09:30

[20] On Nov. 2, the ship conducted a transect across the mouth of Amundsen Gulf. A RADARSAT-1 image was acquired on Nov. 2 at 01:54 (all times herein reported as UTC) just prior to the start of the transect, which clearly

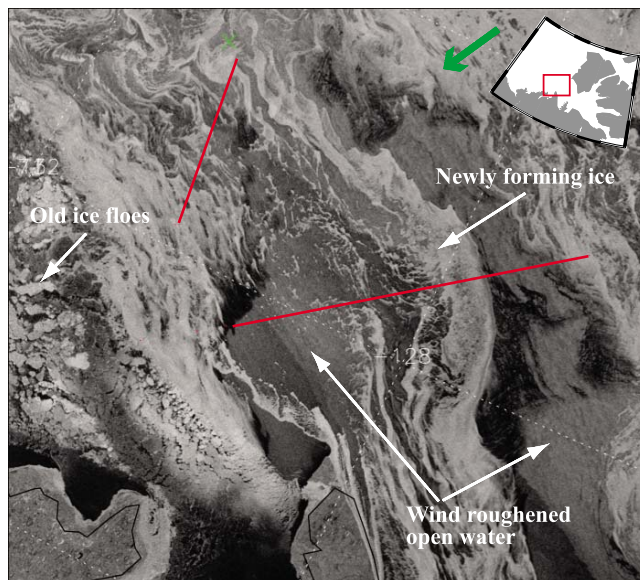


Figure 3. RADARSAT-1 image collected on Nov. 2 at 01:53, just prior to sample case 1. The inset map shows the location of the imaged area, red lines indicate the ship's track, the green X indicates the location of the ship at the time of image acquisition, and the green arrow shows the mean wind direction.

shows that the region was a mix of open water, old ice floes, and newly forming grease ice (Figure 3). Due to the ice in the area the intake line for the $p\text{CO}_{2\text{sw}}$ system was clogged so that we could not obtain measurements of $\Delta p\text{CO}_2$. However, samples collected in the region in the previous two days showed that the $\Delta p\text{CO}_2$ was around $-80 \mu\text{atm}$.

[21] Over this time period, we measured a flux of up to $-4.26 \mu\text{mol m}^{-2} \text{s}^{-1}$, with a mean value of $-1.81 \mu\text{mol m}^{-2} \text{s}^{-1}$. Associated with this strong CO₂ uptake was a high sensible heat flux from the ocean to the atmosphere (up to 100 W m^{-2} , mean of 43.3 W m^{-2} , Figure 4b). This heat flux must have been driven by open water, over which a strong temperature gradient forms due to the relative warmth of the ocean. We therefore interpret the strong CO₂ fluxes to likewise be a signal of open water gas exchange.

4.1.2. Case 3: Nov. 20 01:30–14:45

[22] The second instance where we observed particularly high CO₂ fluxes was on Nov. 20, near the southern tip of Banks Island. At this point ice concentration in Amundsen Gulf was very high, and the ship was parked in a 36 cm thick ice floe. Prior to this time, a strong wind event from Nov. 16–17 (wind velocities peaking at about 24 m s^{-1}) created significant ice motion and fracture in the region. This was followed by very low winds (about 5 m s^{-1}), allowing the open water features to appear obviously on a RADARSAT-1 image acquired on Nov. 20 at 01:29 as dark features (Figure 5). Early on Nov. 20, easterly winds picked up quickly to about 13 m s^{-1} and persisted through the sample case (Figure 6c). This wind induced significant ice motion (the ship drifted at a mean velocity of 0.6 km hr^{-1} , increasing steadily from 0.4 to 1.1 km hr^{-1}), which would have expanded the open water leads. A signal of open-water fluxes was clearly evident in the heat flux measurements,

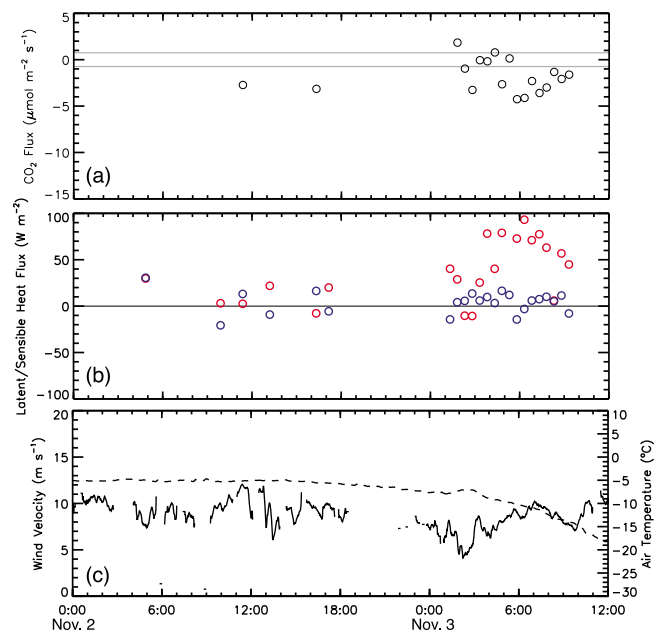


Figure 4. Time series of atmospheric measurements made during sample case 1. (a) Measured CO₂ flux with sensor heating correction added (open circles), and the estimated noise level of the system as discussed in section 5.1 (horizontal grey lines), (b) measured sensible heat flux (red open circles) and latent heat flux (blue open circles), (c) 1 minute averages of air temperature (dashed line) and wind velocity (solid line).

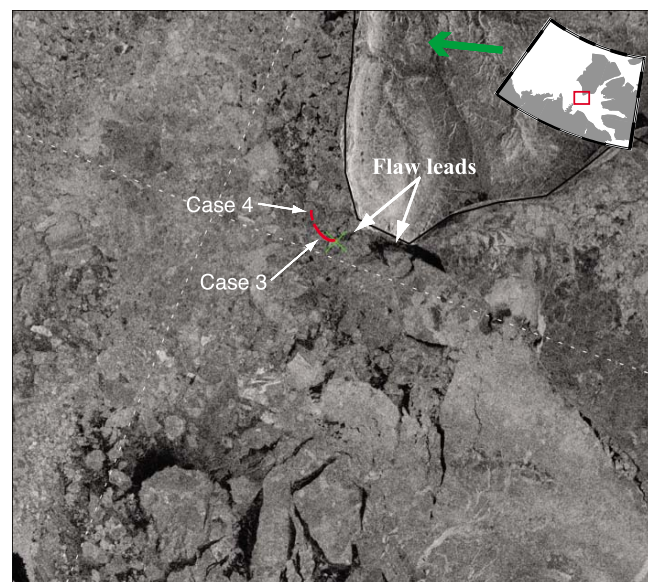


Figure 5. RADARSAT-1 image collected on Nov. 20 at 01:29, just prior to cases 3 and 4. The inset map shows the location of the imaged area, red lines indicate the ship's track, the green X indicates the location of the ship at the time of image acquisition, and the green arrow shows the mean wind direction.

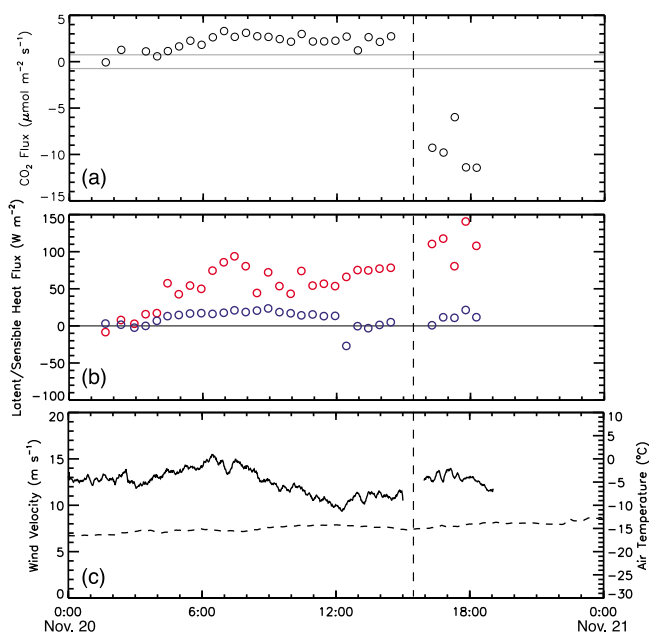


Figure 6. Time series of atmospheric measurements made during sample cases 3 and 4 (division between the two cases is denoted by the dashed vertical line). (a) Measured CO₂ flux with sensor heating correction added (open circles), range of bulk CO₂ flux estimates (brackets), and the estimated detection limit of the system as discussed in section 4.2 (horizontal grey lines), (b) measured sensible heat flux (red open circles) and latent heat flux (blue open circles), (c) 1 minute averages of air temperature (dashed line) and wind velocity (solid line).

reaching nearly $+100 \text{ W m}^{-2}$ (Figure 6b) with a mean value of $+53.8 \text{ W m}^{-2}$ (Table 1).

[23] During this case, rapid outgassing of CO₂ was observed at a mean rate of $+2.10 \mu\text{mol m}^{-2} \text{ s}^{-1}$. The outgassing was somewhat surprising given that the $p\text{CO}_{2\text{sw}}$ system recorded undersaturation of $-75 \mu\text{atm}$ (Table 1), but the surface water upwind of the ship may have been supersaturated. This result shows that at times our eddy covariance measurements (which are an integrated flux from the upwind surfaces) are difficult to reconcile with the $p\text{CO}_{2\text{sw}}$ data (which measures at the same location as the tower).

4.1.3. Case 4: Nov. 20 16:00–18:30

[24] Case 4 is an extension of Case 3, but we split the two because the ship repositioned (approximately 1.5 km north) to a new ice floe (Figure 5), and the CO₂ flux changed markedly. The heat flux measurements from Case 4 were still heavily influenced by an open water signal, with even higher values than in case 3 (mean and maximum values of $+111.4$ and $+140.7 \text{ W m}^{-2}$ respectively, Figure 6b). This is in agreement with ship-board observations that the area was a mixture of ice and open water under strong wind-forcing.

[25] After the ship repositioned, a very strong negative flux of CO₂ was observed (mean and maximum values of -9.58 and $-11.43 \mu\text{mol m}^{-2} \text{ s}^{-1}$ respectively, Figure 6a). This flux direction is in better agreement with the $\Delta p\text{CO}_2$ gradient observed in the area, and may be a result of a change in the upwind surface to lower (i.e. undersaturated)

$p\text{CO}_{2\text{sw}}$ as the ship moved around the southern tip of Banks Island (Figure 5).

4.1.4. Case 7: Dec 1 07:00–12:30

[26] The strongest CO₂ fluxes that we measured were on Dec. 1 during a transit along the southwest coast of Banks Island. Immediately prior to this transit, the ship was drifting south in an ice floe under fairly high winds (mean 11.8 m s^{-1}). This drifting event made up Case 6, where no strong CO₂ fluxes or heat fluxes were observed (Table 1). The ship eventually broke out of this drift, and transited through an active wind-roughened flaw lead. This flaw lead event was captured in a RADARSAT-1 image taken shortly after the end of case 7 (Dec. 1, 14:45, Figure 7).

[27] The transit was very short, and only four 30 minute samples passed our quality control tests. However, all of these samples showed very high CO₂ uptake, with flux values ranging from -9.33 to $-27.95 \mu\text{mol m}^{-2} \text{ s}^{-1}$ (Figure 8a). Once again, these fluxes were accompanied by high sensible heat fluxes indicative of open water (Figure 8b). No $p\text{CO}_{2\text{sw}}$ measurements were available during the transit due to a clogged intake line, but based on the $\Delta p\text{CO}_2$ during the cases bracketing this one (-52.1 and $-63.6 \mu\text{atm}$ for cases 6 and 8, respectively, Table 1), the direction of the flux appeared to be in agreement with the gradient.

4.1.5. Case 17: Jan 24. 08:00–Jan. 25 05:30

[28] The final instance where we measured unusually strong CO₂ fluxes was during case 17 in late January. During this time, the ship was drifting in an ice floe with a thickness of about 100 cm. A RADARSAT image collected at 01:33 on Jan. 24 showed considerable fracturing upwind of the ship (Figure 9).

[29] This case was characterized by high wind velocities (up to 19 m s^{-1} , Figure 10c) which caused ice drift up to

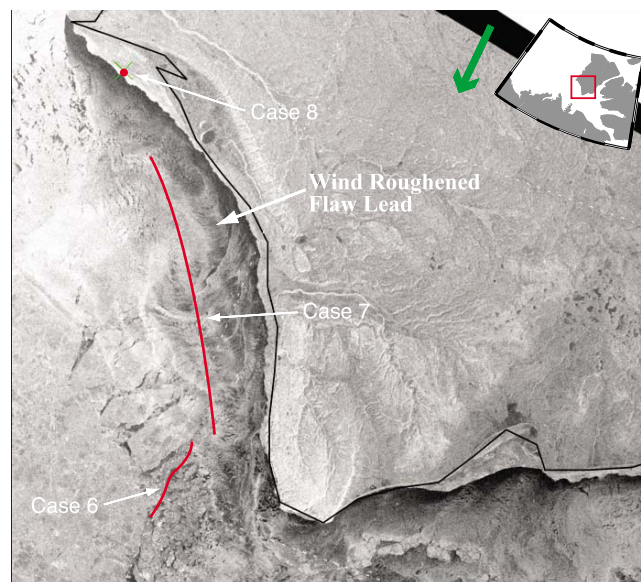


Figure 7. RADARSAT-1 image collected on Dec. 1, 14:45, just after case 7. The inset map shows the location of the imaged area, red lines indicate the ship's track, the green X indicates the location of the ship at the time of image acquisition, and the green arrow shows the mean wind direction.

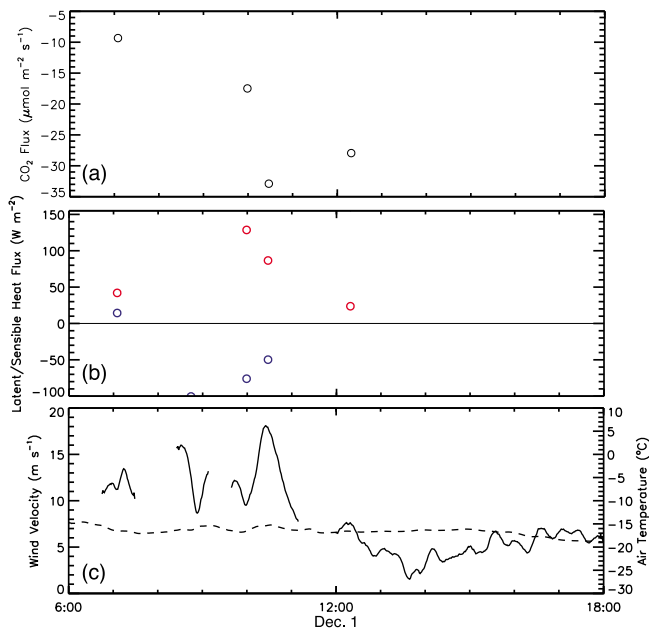


Figure 8. Time series of atmospheric measurements made during sample case 7. (a) Measured CO₂ flux with sensor heating correction added (open circles), and the estimated noise level of the system as discussed in section 5.1 (horizontal grey lines), (b) measured sensible heat flux (red open circles) and latent heat flux (blue open circles), (c) 1 minute averages of air temperature (dashed line) and wind velocity (solid line).

1.4 km hr⁻¹. These strong winds and ice motion drove significant open water, as observed in heat flux measurements approaching 100 W m⁻² (Figure 10b). Associated with this sensible heat signal was a strong, consistent CO₂ uptake (Figure 10a) with a mean flux of $-3.15 \mu\text{mol m}^{-2} \text{s}^{-1}$, in agreement in direction with an observed $\Delta p\text{CO}_2$ gradient of $-38.5 \mu\text{atm}$.

4.2. Observations of Low CO₂ Fluxes

4.2.1. Observations in Land Fast Ice

[30] Flux measurements were made in land fast sea ice on three occasions: case 2 (Nov. 8 02:15–Nov. 9 00:50, 69.50 °N/123.93 °W), case 8 (Dec. 1 13:45–Dec. 2 02:45, 71.90 °N/125.44 °W), and case 11 (Dec. 19 23:15–18:15, 71.91 °N/125.43 °W). The minimum ice thickness for all of these samples was an estimated 40 cm (case 2), and the ice was much thicker (approaching 100 cm) in the other two cases. Sensible heat flux in all cases was small (Table 1), and in all three cases the wind direction was such that the upwind fetch was composed of fast ice. This suggests that what we were measuring was indeed a land fast ice signal. In these cases, mean fluxes were between $+0.23$ – $+0.42 \mu\text{mol m}^{-2} \text{s}^{-1}$ (Table 1 and Figure 2). If these measurements are reliable, they would suggest a flux of CO₂ at a climatologically significant rate. However, we will show in section 5.1 that these low fluxes likely cannot be distinguished from the noise and biases inherent in our eddy covariance system.

4.2.2. Observations in High Concentration Mobile Ice

[31] A second scenario in which we typically observed non-resolvable CO₂ fluxes was when the ship was drifting

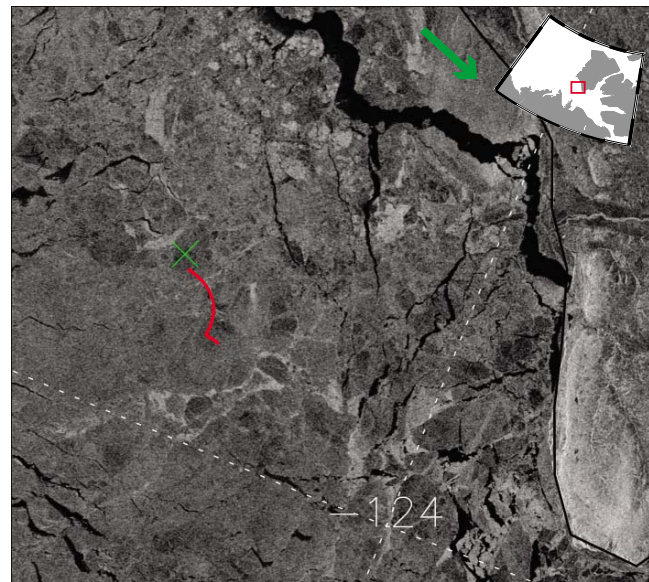


Figure 9. RADARSAT-1 image collected on Jan. 24, 01:33, just prior to case 17. The inset map shows the location of the imaged area, red lines indicate the ship's track, the green X indicates the location of the ship at the time of image acquisition, and the green arrow shows the mean wind direction.

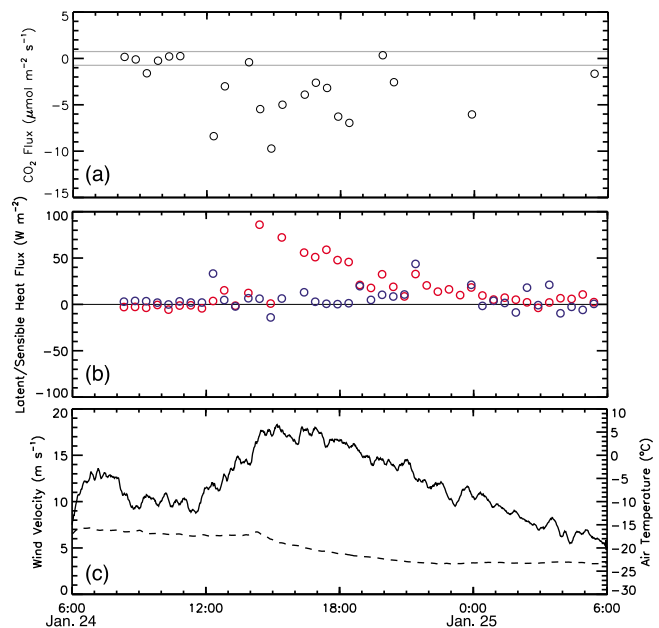


Figure 10. Time series of atmospheric measurements made during sample case 17. (a) Measured CO₂ flux with sensor heating correction added (open circles), and the estimated noise level of the system as discussed in section 5.1 (horizontal grey lines), (b) measured sensible heat flux (red open circles) and latent heat flux (blue open circles), (c) 1 minute averages of air temperature (dashed line) and wind velocity (solid line).

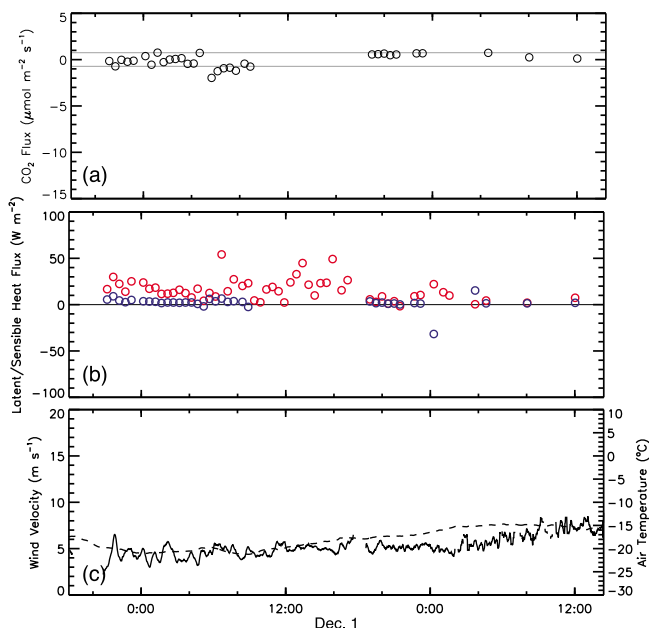


Figure 11. Time series of atmospheric measurements made during sample case 10. (a) Measured CO₂ flux with sensor heating correction added (open circles), and the estimated noise level of the system as discussed in section 5.1 (horizontal grey lines), (b) measured sensible heat flux (red open circles) and latent heat flux (blue open circles), (c) 1 minute averages of air temperature (dashed line) and wind velocity (solid line).

in highly concentrated mobile sea ice. These conditions were observed during case 6 (Nov. 30 05:15–23:00), case 9 (Dec. 2 05:30–22:15), case 13 (Jan. 2 18:15–Jan. 6 03:30), case 14 (Jan. 10 09:15–Jan. 11 18:45), case 15 (Jan. 13 16:00–Jan. 14 00:00) and case 16 (Jan. 20 17:00–Jan. 21 04:30). As Table 1 shows, all of these cases had very low sensible heat fluxes (highest mean flux was $+3.2 \text{ W m}^{-2}$, case 15), and mean CO₂ fluxes ranged from -0.50 – $+0.58 \text{ } \mu\text{mol m}^{-2} \text{ s}^{-1}$ (Table 1 and Figure 2).

4.2.3. Observations in Thin Ice

[32] A final scenario which is perhaps more interesting is the observation of non-detectable CO₂ fluxes in cases where other observations (field data and heat flux measurements) suggest that thin ice may be present. Only case 10 (Dec. 4 23:00–Dec. 6 12:15) falls into this category. RADARSAT-1 images (not shown) acquired shortly before (Dec. 4, 01:21) and after this run (Dec. 7 01:33) do not show a lot of obvious thin ice, but ice cores taken from the surrounding floe were only 26 cm thick. The heat flux measurements (Figure 11b) were consistently positive (mean value of $+15.8 \text{ W m}^{-2}$), but lower than those observed in section 4.1. Thin ice transfers heat at significant rates, but does so less vigorously than open water [Market, 1978]. Although winds were moderate (5 – 7 m s^{-2} , Figure 11c) the $\Delta p\text{CO}_2$ gradient was quite high (mean value of $-86.7 \text{ } \mu\text{atm}$). If a flux enhancement was occurring similar to those described in section 4.1, we would expect to be able to detect it in our CO₂ flux measurements. However, Figure 11a clearly shows that fluxes were not distinctly above the uncertainty inherent in the system. These findings suggest that open water – not

just thin ice – is required to drive CO₂ flux at the levels shown in section 4.1.

5. Discussion

5.1. Sensor Uncertainties

[33] The results obtained in land fast and consolidated ice (sections 4.2.1 and 4.2.2) provide an opportunity to test the noise and bias inherent in our eddy covariance system. There is in fact good reason to expect that CO₂ fluxes over these surfaces (thick, cold, consolidated sea ice) should be zero. At surface ice temperatures below $\sim -5^\circ\text{C}$ and typical brine salinity, the brine volume drops below 5% which inhibits liquid transport through the ice [Golden *et al.*, 1998]. Loose *et al.* [2010] examined the transport of gases near this liquid transport threshold, and found the gas transfer velocity to be very small relative to seawater. Similarly, Nomura *et al.* [2006] measured small CO₂ fluxes (maximum $\sim +0.01 \text{ } \mu\text{mol m}^{-2} \text{ s}^{-1}$) over thin laboratory ice well above the liquid transport threshold. At ice temperatures that reduce brine volume to below 5%, these small rates of gas exchange should be effectively shut off.

[34] After Nov. 28, 2007 (when most of the measurements described in sections 4.2.1 and 4.2.2 were made) surface ice temperatures were consistently well below -5°C and brine volumes were typically below 5% (G. Carnat, unpublished data, 2007). We would therefore expect any deviation of the mean CO₂ fluxes over these surfaces from zero to be indicative of bias, and any variation around that mean to be noise in the measurement system. To this end, we calculated the mean and standard deviation of the raw, sensor heating corrected, and crosstalk (PKT) corrected CO₂ fluxes from cases 2, 6, 8, 9, 11 and 13–16 (Table 2).

[35] The uncorrected fluxes show a negative bias ($-0.45 \text{ } \mu\text{mol m}^{-2} \text{ s}^{-1}$), which is in the direction predicted by both sensor heating and water vapor crosstalk effects. The standard deviation of CO₂ fluxes around this mean was $0.76 \text{ } \mu\text{mol m}^{-2} \text{ s}^{-1}$, indicating that noise is quite high in the system. By applying only the sensor heating correction, the bias moved to $+0.13 \text{ } \mu\text{mol m}^{-2} \text{ s}^{-1}$ – a reduction in the magnitude of the bias, but a slight overcorrection. Fortunately, this correction did not add a lot of additional noise to the system, as the standard deviation remained relatively unchanged ($0.77 \text{ } \mu\text{mol m}^{-2} \text{ s}^{-1}$).

[36] The PKT correction, however, was more troublesome. We found that 55% of the samples from these cases produced what we determined to be an “unreasonable” correction (magnitude of correction $>5.5 \text{ } \mu\text{mol m}^{-2} \text{ s}^{-1}$). Of the remaining samples, the net effect of the correction was to

Table 2. Noise and Bias in the Eddy Covariance System, Including the Effect of Various Corrections^a

	Bias ($\mu\text{mol m}^{-2} \text{ s}^{-1}$)	Noise ($\mu\text{mol m}^{-2} \text{ s}^{-1}$)
Raw (uncorrected)	-0.45	± 0.76
Sensor heating corrected	0.13	± 0.77
Water vapor crosstalk correction	-0.21	± 1.32

^aBias is calculated as the mean CO₂ flux from cases where near-zero flux is expected, noise is one standard deviation around that mean. The number of eddy covariance sample runs is 274 for raw and sensor heating corrected, 151 for crosstalk corrected.

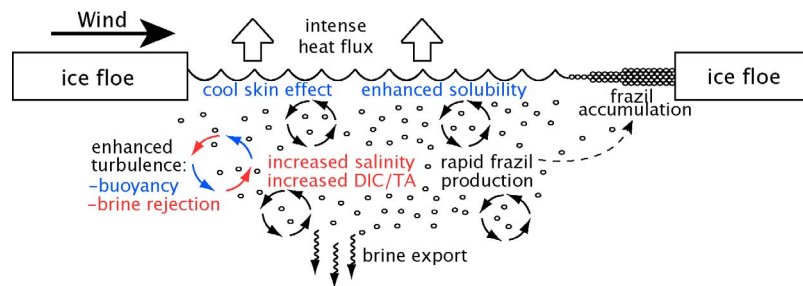


Figure 12. Schematic summarizing the important processes occurring during a wind-driven lead event. The processes highlighted in blue/red are those which likely have a direct effect on air-sea gas exchange. Processes in red are associated with frazil ice formation, and those in blue are associated with the surface cooling.

actually make the CO₂ flux more negative, counter to the expected direction. Furthermore, the correction added additional noise as evidenced by an increase in standard deviation to $1.30 \mu\text{mol m}^{-2} \text{s}^{-1}$. Since no negative bias remains in the mean flux after the sensor heating correction, we conclude that crosstalk contamination must have been small for our system even prior to applying the PKT correction. Arguments for a low crosstalk error in this environment have a strong physical basis, because latent heat fluxes were very small (typically $<5 \text{ W m}^{-2}$) compared to the examples discussed by Prytherch *et al.* [2010] ($\sim 60 \text{ W m}^{-2}$). From an eddy covariance standpoint, a low latent heat flux means that water vapor is not highly correlated with vertical wind velocity, and thus should not cause significant spurious correlation between CO₂ and vertical wind velocity. For these reasons, we decided not to include the PKT correction in our results.

[37] We propose that our system has an overall uncertainty of $\pm 0.77 \mu\text{mol m}^{-2} \text{s}^{-1}$ and a bias of $+0.13 \mu\text{mol m}^{-2} \text{s}^{-1}$ based on the results of the sensor heating corrected fluxes. This level of uncertainty shows that our measurements of high CO₂ flux (section 4.1) are above the noise level of the system, and are not the result of a strong systematic bias.

5.2. Enhanced Gas Flux by Sea Ice Formation

[38] Our results from section 4.1 indicate that in the winter mixed ice environment of the Amundsen Gulf, the presence of open water drives a very rapid exchange of CO₂. For comparison, under the typical $\Delta p\text{CO}_2$ ($\sim 70 \mu\text{atm}$) and wind velocity ($\sim 8 \text{ m s}^{-1}$) conditions we encountered, the bulk flux approach (equation (1)) would predict fluxes in the range of -0.10 to $-0.12 \mu\text{mol m}^{-2} \text{s}^{-1}$. Even using the maximum wind velocities observed (19 m s^{-1}), we would not expect fluxes to exceed about $-1.5 \mu\text{mol m}^{-2} \text{s}^{-1}$. Our measured fluxes are therefore at times 1–2 orders of magnitude higher than what might be expected under similar conditions in the open ocean.

[39] Several authors have suggested that an enhancement of gas exchange due to sea ice formation may exist [Anderson *et al.*, 2004; Rysgaard *et al.*, 2007; Loose *et al.*, 2009], but none have described in detail the physical and chemical processes which may account for it. Our study likewise lacks the necessary ancillary observations to show conclusively what processes are responsible for enhanced gas transfer, but in this section we propose two key hypotheses to explain it: (1) enhanced water side turbulence driven by

rapid cooling and brine rejection, and (2) modification of the carbonate system of the surface seawater. These hypotheses are summarized in Figure 12 and discussed below.

5.2.1. Enhanced Water Side Turbulence

[40] At the upwind side of a flaw lead, a significant heat flux occurs due to the exposure of the relatively warm (i.e. $\sim 1.8 \text{ }^\circ\text{C}$) water to the very cold atmosphere (~ -10 – $-25 \text{ }^\circ\text{C}$). This cooling creates a destabilization of the water surface and generates buoyancy fluxes that may enhance turbulence. McGillis *et al.* [2004] observed a 40% enhancement of CO₂ fluxes during modest nighttime cooling (sensible heat fluxes on the order of 1 – 10 W m^{-2}) in the equatorial Pacific, which was attributed mostly to these buoyancy fluxes. In a situation such as the one shown in Figure 12 where sensible heat fluxes are 1–2 orders of magnitude higher, this enhancement is likely to be much more pronounced.

[41] A second process that may drive high turbulence is the rejection of dense brines by frazil ice formation. Frazil ice is small, unconsolidated ice crystals that are primarily generated just below the surface [Ushio and Wakatsuchi, 1993]. It is easily transported away from the open water site, creating a region of rapid ice formation but persistent open water. Frazil ice crystals are thought to be essentially pure [Omstedt, 1985] which means that their formation results in the rejection of any solutes, which must create density instabilities and drive enhanced turbulence similar to the effect of heat loss.

[42] Unfortunately, turbulence in these systems has not been well studied. Between Nov. 16–Dec. 18, one of our collaborators collected 175 profiles of turbulent kinetic energy dissipation rate (ϵ) from a minimum depth of 10 m using a vertical microstructure turbulence profiler (VMP, see Bourgault *et al.* [2008] for instrument details). ϵ at 10 m reached values of $O(10^{-5}) \text{ W kg}^{-1}$ on a few (~ 4) profiles, with an approximately exponential decrease with depth [Bourgault *et al.*, 2011]. Extrapolating above 10 m suggests surface dissipation rates that may have occasionally reached $O(10^{-4}) \text{ W kg}^{-1}$. These values are considerably higher than ϵ measured under refrozen leads at a similar depth by McPhee and Stanton [1996] ($O(10^{-8})$ – $O(10^{-7}) \text{ W kg}^{-1}$). The exponential shape of the dissipation measurements points to surface turbulence generation, but given that the dominant ice cover must restrict wind and wave action, sea ice processes (likely including ice drift and brine rejection) must play an important role in this system. Zappa *et al.* [2007] showed that ϵ is a better predictor of gas transfer

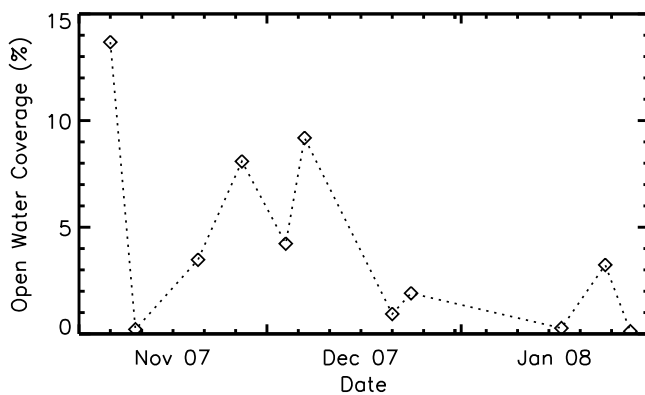


Figure 13. Open water percentage for Amundsen Gulf (122–126°W, 70–71.5°N) during the study period, as determined by classification of near-weekly RADARSAT-1 imagery.

velocity than wind in systems where turbulence is generated from other sources. Our maximum predicted surface ϵ values are similar to the highest ϵ measurements made by Zappa *et al.* [2007] in coastal zones and tidal estuaries, but they are not high enough to account for the rate of gas transfer we observed. However, the VMP was almost always deployed when the ship was stationary in ice floes, and it therefore may not have captured the nature of the transient flow leads that we hypothesize to be the cause of our high observed CO₂ fluxes.

5.2.2. Modification of the Surface Seawater Carbonate System

[43] $p\text{CO}_{2,\text{sw}}$ is ultimately controlled by the equilibrium condition of the seawater carbonate system. DIC, TA, salinity and water temperature all affect this equilibrium, and thus exert a control on $p\text{CO}_{2,\text{sw}}$. In terms of gas exchange, it is actually the carbonate system properties of the very thin mass diffusive layer that determines the air-sea $\Delta p\text{CO}_2$.

[44] The most obvious modification by lead formation is cooling of the sea surface, which will reduce $p\text{CO}_{2,\text{sw}}$ and increase solubility. Although the seawater will be near its freezing point, cooling beyond the freezing point (supercooling) occurs before ice formation begins. If no particles are available for the nucleation of ice crystals, supercooling can easily exceed 2° C [Tsang and Hanley, 1985]; a condition which can be created in the laboratory, but is not likely to exist in the Arctic. Observations of supercooling in the field are sparse, but Skogseth *et al.* [2009] observed a supercooling of ~0.04 °C in the bulk surface water of an open coastal polynya in Svalbard. Given that the heat loss is at the surface, this would likely translate into an even more significant cooling of the diffusive mass boundary layer – in essence, the rapid sensible heat flux would drive a very pronounced cool-skin effect. This cool-skin effect would enhance uptake when the sea surface was undersaturated due to increased solubility and decreased $p\text{CO}_{2,\text{sw}}$, but would actually act to restrict exchange when the surface was supersaturated. Given that we measured one instance of intense outgassing (case 3, section 4.1.2), this process alone cannot account for the high exchange rates.

[45] Frazil ice formation and the accompanying rejection of brines also has the potential to modify the near-surface

chemistry. A decrease in solubility driven by salt rejection and rising DIC/TA concentrations may either suppress or enhance gas exchange, depending on the saturation state. When the sea surface is supersaturated, the added DIC/TA and reduced solubility should enhance outgassing. When the sea surface is undersaturated, these combined effects should suppress uptake. However, whether or not this has an influence on gas exchange depends on where the brines ultimately end up. On the nearby Beaufort Sea Shelf, Melling and Moore [1995] showed that deep penetration to the pycnocline of brine does occur at times, which suggests that modification of the near-surface chemistry may not be important. Shadwick *et al.* [2011] did measure long-term surface increases in salinity, and DIC/TA in Amundsen Gulf over the winter, but we do not have measurements that capture the evolution of these properties on the timescale of an individual flaw lead event. On these short timescales, we hypothesize that the effects of brine rejection will be minor. Since most of the frazil ice formation is occurring below the ocean skin, there will not be much immediate modification of the chemistry of the mass diffusive layer. Ushio and Wakatsuchi [1993] also showed that the brine rejection from frazil crystals is concentrated in thin streamers that rapidly descend downward. If leads are small and short-lived, there would be a significant amount of unmodified water available laterally and vertically to replace those descending brines, keeping the surface water properties near-constant.

[46] Ultimately, we cannot draw any firm conclusions regarding the short timescale modifications to the seawater carbonate system. However, given the manner in which the carbonate system is entwined with many of the processes that occur with lead formation, this should be a major focus of future studies.

5.3. Significance to the Amundsen Gulf Region

[47] The total winter CO₂ flux through open water in the Amundsen Gulf depends on not only the rate at which it occurs, but also on the areal extent of open water. In this section, we combine estimates of these two variables for the purpose of computing area-averaged fluxes. By calculating these fluxes, we can estimate the significance of winter CO₂ exchange relative to the open water season (i.e. late spring/summer/early fall), and we can determine if the fluxes are reasonable based on the water column DIC budget for the region devised by Shadwick *et al.* [2011].

[48] As described in section 3.5, we used RADARSAT-1 imagery to estimate the open water fraction in a bounding box (122–126°W, 70–71.5°N) consistent with the one used by Shadwick *et al.* [2011]. RADARSAT-1 images that captured this area were available approximately every week, and the open water fraction calculated for each image are shown in Figure 13. The amount of open water during the study was highly variable, which probably relates to storm events in the area. To allow comparisons with the results of Shadwick *et al.* [2011], monthly averages of open water fraction were calculated, and are displayed in Table 3.

[49] To estimate the rate of gas exchange over the area we would ideally have some way of scaling our flux measurements using $\Delta p\text{CO}_2$ and an easily-obtainable variable like wind speed, but at this point our data set is too limited to work toward parameterization. Therefore, we simply cal-

Table 3. Summary of Monthly Lead Fraction, CO₂ Fluxes and Resulting Change in Mixed Layer DIC

	November	December	January
Mean Open Water ^a (%)	6.4	4.1	1.2
$F_{CO_2sw-mon}$ ^b ($\mu\text{mol m}^{-2} \text{s}^{-1}$)	-0.3	-0.2	-0.1
$\Delta\text{DIC}_{as-enh}$ ^c ($\mu\text{mol kg}^{-1}$)	16.2	10.7	3.1
ΔDIC_{as} ^d ($\mu\text{mol kg}^{-1}$)	1	2	0.1
ΔDIC_{bio} ^e ($\mu\text{mol kg}^{-1}$)	3.0 ± 10.0	13.0 ± 10.0	16.0 ± 10.0

^aCalculated from RADARSAT-1 image classification.

^bCalculated from mean of cases 1, 4, 7 & 17, multiplied by lead fraction and integrated over the month.

^cCalculated change in DIC concentration over a 50 m mixed-layer using $F_{CO_2sw-mon}$.

^dCalculated change in DIC concentration over a 50 m mixed-layer using bulk-flux estimates scaled for open water fraction [from *Shadwick et al.*, 2011].

^eCalculated change in DIC concentration over a 50 m mixed layer due to biological activity [from *Shadwick et al.*, 2011].

culated the mean uptake rate from cases 1,4,7 and 17 (those with substantial uptake; the outgassing observed during case 3 was omitted because the offshore Amundsen Gulf was undersaturated through the entire winter [*Shadwick et al.*, 2011]) to be $-4.88 \mu\text{mol m}^{-2} \text{s}^{-1}$. This rate was multiplied by the average monthly open water fraction to calculate the mean monthly fluxes shown in Table 3.

[50] To address the question of whether these fluxes are reasonable we integrated the flux over each month, and calculated the net change in DIC (denoted $\Delta\text{DIC}_{as-enh}$ in Table 3) that would occur assuming a 50m mixed-layer depth. *Shadwick et al.* [2011] budgeted month-by-month changes in DIC in the Amundsen Gulf mixed layer via:

$$\Delta\text{DIC}_{obs} = \Delta\text{DIC}_{bio} + \Delta\text{DIC}_{fw} + \Delta\text{DIC}_{as} + \Delta\text{DIC}_{vd} \quad (3)$$

where ΔDIC_{obs} was the observed monthly change in DIC, and the right hand terms are monthly changes in DIC due to biological activity (ΔDIC_{bio}), freshwater fluxes (ΔDIC_{fw}), air-sea exchange (ΔDIC_{as}) and vertical diffusion (ΔDIC_{vd}). ΔDIC_{fw} and ΔDIC_{vd} were calculated from in situ data, and ΔDIC_{as} was calculated using a bulk flux approach scaled for ice concentration. No direct method was available to measure the biological contribution, so it was calculated as a difference of the 4 other terms. With no other constraint on the biological contribution to ΔDIC_{obs} , a flux of CO₂ which is enhanced beyond ΔDIC_{as} would be mis-allocated into ΔDIC_{bio} . Thus if our calculated $\Delta\text{DIC}_{as-enh}$ fits within the sum of ΔDIC_{as} and ΔDIC_{bio} it can be considered to fit in the budget. Table 3 shows that this is the case in all months under consideration, except November. This shows that although the fluxes associated with this enhanced air-sea exchange are very high, they are not unrealistic from the standpoint of the DIC budget.

[51] With respect to significance for the Amundsen Gulf region, the fluxes calculated accounting for enhanced air-sea exchange are more than an order of magnitude higher than those calculated by *Shadwick et al.* [2011] using a bulk flux approach scaled for ice concentration (Table 3). In fact, these fluxes place the air-sea exchange rates on par with the open water season rates calculated by *Shadwick et al.* [2011]. This is a significant consideration, because the typical model of a polynya's annual air-sea budget is characterized by open water uptake during the autumn storm season (utilizing

an initial biological $p\text{CO}_{2sw}$ drawdown in the spring) which is then capped by ice over the winter [*Yager et al.*, 1995]. The strength of annual uptake by a polynya was thought to be constrained by whether or not the spring undersaturation could be utilized by open water air-sea exchange, but the results from this study show that uptake may proceed beyond ice formation. It should be noted, however, that not every polynya may remain undersaturated through the winter; in polynyas where this is not the case, winter outgassing through open water may tip the annual balance away from net uptake.

5.4. Potential Significance to the Arctic Ocean

[52] As well as creating a need to re-think the seasonal evolution of gas exchange for polynyas, enhanced winter gas exchange may play an important role in the broader Arctic and Antarctic Oceans. *Omar et al.* [2005] used a simple extrapolation of winter air-sea CO₂ exchange estimated in Storfjorden to show that Arctic polynyas are likely a significant sink for atmospheric CO₂. Our study confirms that at least one other Arctic polynya behaves as they predict, an important step in validating their larger scale estimates. In addition to polynyas, we hypothesize that flaw leads may act as important centers for winter gas exchange. Leads are typically a small fraction of the Arctic icescape during winter; *Lindsay and Rothrock* [1995] estimated the percentage to be 2–3% for the central Arctic and 6–9% for the peripheral seas. However, our findings suggest that even at low fractions these features may dominate the winter gas exchange budget much in the same way that they dominate heat fluxes [*Maykut*, 1978; *Andreas*, 1980]. Also of note are the large areas of the Arctic and Antarctic ocean which are seasonally ice-free. In the Arctic, this makes up an area of $6.4 \times 10^6 \text{ km}^2$ and in the Antarctic $15.2 \times 10^6 \text{ km}^2$ [*Wadhams*, 2000] (1979–87 averages). As discussed by *Omar et al.* [2005], the seasonal formation of sea ice over these areas may create short but intense CO₂ fluxes which could be important to the annual air-sea CO₂ exchange budget of the Arctic and Southern Oceans.

[53] Ongoing and anticipated changes in the polar oceans may further increase the importance of this effect. The rapidly decreasing summer ice extent in the Arctic [e.g., *Stroeve et al.*, 2007] means that a larger area will be subject to annual ice formation, and significant positive trends in sea ice motion [*Hakkinen et al.*, 2008] may create more wintertime open water. Our results show that this will permit larger annual air-sea gas exchange, but whether this will result in a larger net sink of CO₂ is complicated. Surface seawater that is undersaturated in $p\text{CO}_{2sw}$ can only absorb a finite amount of CO₂, depending on the state of the carbonate equilibrium (i.e. the Revelle factor). A debate is currently emerging regarding whether the ocean surface exposed by recent sea ice loss has the capacity to take up significant amounts of CO₂ [*Bates et al.*, 2006; *Cai et al.*, 2010]. A similar debate needs to be had regarding uptake capacity of the Arctic Ocean at freezeup in order to understand the potential for gas exchange enhanced by ice formation. A net annual sink also requires export of absorbed CO₂ to depth, a process that appears to occur effectively on the shelves where deep water formation occurs but not necessarily in the Arctic Ocean basins [*Omar et al.*, 2005]. Clearly, a lot of work remains to be done before we can fully

understand the interplay between enhanced gas exchange and future changes to the Arctic Ocean.

6. Summary and Conclusions

[54] This paper has provided the first direct, in situ observations of enhanced gas exchange during sea ice formation. Eddy covariance calculations of CO₂ flux in Amundsen Gulf (a polynya with a dynamic winter sea ice cover) showed periods of intense uptake (mean flux -4.88 , maximum $-27.95 \mu\text{mol m}^{-2} \text{s}^{-1}$) and one case of outgassing (mean flux $+2.10 \mu\text{mol m}^{-2} \text{s}^{-1}$). These periods of high gas exchange were observed coincidentally with high heat fluxes, which we confirmed from satellite imagery to be the result of open water (i.e. flaw leads). Conversely, we measured no fluxes above the uncertainty of our instruments over consolidated sea ice.

[55] We presented several hypotheses to explain our observations of enhanced gas transfer. In a winter flaw lead, we expect high water-side turbulence to occur as a result of rapid heat loss and salt rejection. Since turbulence is the first-order control on gas exchange, we hypothesize that this high turbulence is a major cause of enhanced gas exchange. We also discussed the modification of surface properties (temperature, salinity, DIC/TA) and their effect on the seawater carbonate system. The potential of these modifications to influence the rate of gas exchange depends on the saturation state of CO₂ with respect to the atmosphere, and at times may actually be contradictory to high fluxes. In support of these hypotheses, we were only able to provide limited evidence of high turbulence in the region.

[56] By comparing our flux values with DIC measurements we were able to show that although high, they do fit within surface DIC budgets. A rough calculation of the integrated CO₂ uptake over the months of Nov.–Jan. showed that winter gas exchange may in fact be as important as the open water (i.e. late spring/summer/early fall) seasons. These results have wide reaching implications for understanding the annual air-sea CO₂ budgets of polynyas and other seasonally ice-free seas.

[57] **Acknowledgments.** Thank you to the Captains and crew of the *CCGS Amundsen* and the many people who helped in the field: Bruce Johnson, Sarah Woods, Kyle Swystun, Gauthier Carnat, Elizabeth Shadwick, Keith Johnson, Jens Ehn, Silvia Gremes-Cordero, Sylvain Blondeau, Luc Michaud and many others. Thank you to John Prytherch, whose help with the PKT correction is greatly appreciated. We also acknowledge the thoughtful input of two anonymous reviewers who greatly improved the manuscript. This work is a contribution to the International Polar Year-Circumpolar Flaw Lead System Study (IPY-CFL 2008), supported by the Canadian IPY Federal program office, the Natural Sciences and Engineering Research Council (NSERC) and many other contributors. The authors of this paper are members of ArcticNet, funded in part by the Networks of Centres of Excellence Canada, NSERC, the Canadian Institute of Health Research and the Social Sciences and Humanities Research Council. B. Else is supported by a Vanier Canada Graduate Scholarship, and received funding for logistics from the Northern Scientific Training Program. W.D. acknowledges support from NASA grant NNX07AR22G. We gratefully acknowledge the continued support of the Centre for Earth Observation Science and the University of Manitoba.

References

Amiro, B. (2010), Estimating annual carbon dioxide eddy fluxes using open-path analysers for cold forest sites, *Agric. For. Meteorol.*, *150*(10), 1366–1372, doi:10.1016/j.agrformet.2010.06.007.

Antil, F., M. A. Donelan, W. M. Drennan, and H. C. Graber (1994), Eddy-correlation measurements of air-sea fluxes from a discus buoy, *J. Atmos. Oceanic Technol.*, *11*, 1144–1150.

Anderson, L. G., E. Falck, E. P. Jones, S. Jutterström, and J. H. Swift (2004), Enhanced uptake of atmospheric CO₂ during freezing of seawater: A field study in Storfjorden, Svalbard, *J. Geophys. Res.*, *109*, C06004, doi:10.1029/2003JC002120.

Andreas, E. L. (1980), Estimation of heat and mass fluxes over arctic leads, *Mon. Weather Rev.*, *108*, 2957–2063.

Asher, W. E., L. M. Karle, B. J. Higgins, P. J. Farley, E. C. Monahan, and I. S. Leife (1996), The influence of bubble plumes on air-seawater gas transfer velocities, *J. Geophys. Res.*, *101*(C5), 12,027–12,041, doi:10.1029/96JC00121.

Bates, N. R., S. B. Moran, D. A. Hansell, and J. T. Mathis (2006), An increasing CO₂ sink in the Arctic Ocean due to sea-ice loss, *Geophys. Res. Lett.*, *33*, L23609, doi:10.1029/2006GL027028.

Bock, E. J., T. Hara, N. M. Frew, and W. R. McGillis (1999), Relationship between air sea gas transfer and short wind waves, *J. Geophys. Res.*, *104*(C11), 25,821–25,831, doi:10.1029/1999JC900200.

Bolin, B. (1960), On the exchange of carbon dioxide between the atmosphere and the sea, *Tellus*, *12*(3), 274–281.

Bourgault, D., D. E. Kelley, and P. S. Galbraith (2008), Turbulence and boluses on an internal beach, *J. Mar. Res.*, *66*, 563–588.

Bourgault, D., C. Hamel, F. Cyr, J.-É. Tremblay, P. S. Galbraith, D. Dumont, and Y. Gratton (2011), Turbulent nitrate fluxes in the Amundsen Gulf during ice-covered conditions, *Geophys. Res. Lett.*, *38*, L15602, doi:10.1029/2011GL047936.

Burba, G. G., D. K. McDermitt, A. G. Grelle, D. J. Anderson, and L. Xu (2008), Addressing the influence of instrument surface heat exchange on the measurements of CO₂ flux from open-path gas analyzers, *Global Change Biol.*, *14*(8), 1854–1876, doi:10.1111/j.1365-2486.2008.01606.x.

Cai, W., et al. (2010), Decrease in the CO₂ uptake capacity in an ice-free Arctic Ocean basin, *Science*, *329*(5991), 556–559.

Canadian Ice Service (2002), MANICE: Manual of standard procedures for observing and reporting ice conditions, 9th edition, Environ. Can., Ottawa, Ontario, Canada.

Denman, K., et al. (2007), Couplings between changes in the climate system and biogeochemistry, in *Climate Change 2007: The Physical Science Basis. Contribution of Working Group I to the Fourth Assessment Report of the Intergovernmental Panel on Climate Change*, edited by S. Solomon et al., chap. 7, pp. 499–587, Cambridge Univ. Press, Cambridge, U. K.

Dugan, J. P., S. L. Panichas, and R. L. DiMarco (1991), Decontamination of wind measurements from buoys subjected to motions in a seaway, *J. Atmos. Oceanic Technol.*, *8*, 85–95.

Edson, J. B., A. A. Hinton, K. E. Prada, J. E. Hare, and C. W. Fairall (1998), Direct covariance flux estimates from mobile platforms at sea, *J. Atmos. Oceanic Technol.*, *15*, 547–562, doi:10.1175/1520-0426(1998)015.

Frew, N. M. (1997), The role of organic films in air-sea gas exchange, in *The Sea Surface and Global Change*, edited by P. S. Liss and R. A. Duce, pp. 121–173, Cambridge Univ. Press, Cambridge, U. K.

Frew, N. M., et al. (2004), Air-sea gas transfer: Its dependence on wind stress, small-scale roughness, and surface films, *J. Geophys. Res.*, *109*(C8), C08S17, doi:10.1029/2003JC002131.

Fujitani, T. (1981), Direct measurement of turbulent fluxes over the sea during AMTEX, *Pap. Meteorol. Geophys.*, *32*(3), 119–134.

Galley, R. J., E. Key, D. G. Barber, B. J. Hwang, and J. K. Ehn (2008), Spatial and temporal variability of sea ice in the southern Beaufort Sea and Amundsen Gulf: 1980–2004, *J. Geophys. Res.*, *113*(C5), C05S95, doi:10.1029/2007JC004553.

Golden, K., S. Ackley, and V. Lytle (1998), The percolation phase transition in sea ice, *Science*, *282*(5397), 2238–2241.

Gosink, T. A., J. G. Pearson, and J. J. Kelley (1976), Gas movement through sea ice, *Nature*, *263*, 41–42, doi:10.1038/263041a0.

Hakkinen, S., A. Proshutinsky, and I. Ashik (2008), Sea ice drift in the Arctic since the 1950s, *Geophys. Res. Lett.*, *35*, L19704, doi:10.1029/2008GL034791.

Hirata, R., T. Hirano, N. Saigusa, Y. Fujinuma, K. Inukai, Y. Kitamori, Y. Takahashi, and S. Yamamoto (2007), Seasonal and interannual variations in carbon dioxide exchange of a temperate larch forest, *Agric. For. Meteorol.*, *147*(3–4), 110–124, doi:10.1016/j.agrformet.2007.07.005.

Ho, D. T., C. J. Zappa, W. R. McGillis, L. F. Bliven, B. Ward, J. W. Dacey, P. Schlosser, and M. B. Hendricks (2004), Influence of rain on air-sea gas exchange: Lessons from a model ocean, *J. Geophys. Res.*, *109*, C08S18, doi:10.1029/2003JC001806.

Ho, D. T., C. S. Law, M. J. Smith, P. Schlosser, M. Harvey, and P. Hill (2006), Measurements of air-sea gas exchange at high wind speeds in the Southern Ocean: Implications for global parameterizations, *Geophys. Res. Lett.*, *33*, L16611, doi:10.1029/2006GL026817.

- Jähne, B. (1987), On the parameters influencing air-water gas exchange, *J. Geophys. Res.*, 92(C2), 1937–1950, doi:10.1029/JC092iC02p01937.
- Järvi, L., I. Mammarella, W. Eugster, A. Ibrom, E. Siivola, E. Dellwik, P. Keronen, G. Burba, and T. Vesala (2009), Comparison of net CO₂ fluxes measured with open- and closed-path infrared gas analyzers in an urban complex environment, *Boreal Environ. Res.*, 14, 499–514.
- Kaimal, J. C., and J. E. Gaynor (1991), Another look at sonic thermometry, *Boundary Layer Meteorol.*, 56, 401–410.
- Kohsiek, W. (2000), Water vapor cross-sensitivity of open path H₂O/CO₂ sensors, *J. Atmos. Oceanic Technol.*, 17, 299–311.
- Körtzinger, A., H. Thomas, B. Schneider, N. Gronau, L. Mintrop, and J. C. Duinker (1996), At-sea intercomparison of two newly designed underway pCO₂ systems—encouraging results, *Mar. Chem.*, 52(2), 133–145, doi:10.1016/0304-4203(95)00083-6.
- Kuss, J., and B. Schneider (2004), Chemical enhancement of the CO₂ gas exchange at a smooth seawater surface, *Mar. Chem.*, 91(1–4), 165–174, doi:10.1016/j.marchem.2004.06.007.
- Leuning, R. (2004), Measurements of trace gas fluxes in the atmosphere using eddy covariance: WPL corrections revisited, in *Handbook of Micrometeorology: A Guide to Surface Flux Measurement and Analysis*, edited by X. Lee, W. J. Massman, and B. E. Law, pp. 119–132, Kluwer Acad., Boston, Mass.
- Lindsay, R. W., and D. A. Rothrock (1995), Arctic sea ice leads from advanced very high resolution radiometer images, *J. Geophys. Res.*, 100(C3), 4533–4544, doi:10.1029/94JC02393.
- Liss, P. S., and L. Merlivat (1986), Air-sea gas exchange rates: Introduction and synthesis, in *The Role of Air-Sea Exchange in Geochemical Cycling*, edited by P. Buat-Menard, pp. 113–127, D. Reidel, Boston, Mass.
- Loose, B., W. R. McGillis, P. Schlosser, D. Perovich, and T. Takahashi (2009), Effects of freezing, growth, and ice cover on gas transport processes in laboratory seawater experiments, *Geophys. Res. Lett.*, 36(5), L05603, doi:10.1029/2008GL036318.
- Loose, B., P. Schlosser, D. Perovich, D. Ringelberg, D. Ho, T. Takahashi, J. Richter-Menge, C. Reynolds, W. McGillis, and J.-L. Tison (2010), Gas diffusion through columnar laboratory sea ice: Implications for mixed layer ventilation of CO₂ in the seasonal sea ice zone, *Tellus, Ser. B*, 23–39, doi:10.1111/j.1600-0889.2010.00506.x.
- Maykut, G. A. (1978), Energy exchange over young sea ice in the Central Arctic, *J. Geophys. Res.*, 83(C7), 3646–3658, doi:10.1029/JC083iC07p03646.
- McGillis, W. M., J. B. Edson, J. E. Ware, J. H. W. Dacey, J. E. Hare, C. W. Fairall, and R. Wanninkhof (2001), Carbon dioxide flux techniques performed during GasEx-98, *Mar. Chem.*, 75, 267–280, doi:10.1016/S0304-4203(01)00042-1.
- McGillis, W. R., et al. (2004), Air-sea CO₂ exchange in the equatorial Pacific, *J. Geophys. Res.*, 109, C08S02, doi:10.1029/2003JC002256.
- McPhee, M. G., and T. P. Stanton (1996), Turbulence in the statically unstable oceanic boundary layer under arctic leads, *J. Geophys. Res.*, 101(C3), 6409–6428.
- Melling, H., and R. Moore (1995), Modification of halocline source waters during freezing on the Beaufort Sea shelf: Evidence from oxygen isotopes and dissolved nutrients, *Cont. Shelf Res.*, 15(1), 89–113.
- Mucci, A., B. Lansard, L. A. Miller, and T. N. Papakyriakou (2010), CO₂ fluxes across the air-sea interface in the southeastern Beaufort Sea: Ice-free period, *J. Geophys. Res.*, 115, C04003, doi:10.1029/2009JC005330.
- Mitsuta, Y., and T. Fujitani (1974), Direct measurement of turbulent fluxes on a cruising ship, *Boundary Layer Meteorol.*, 6, 203–217, doi:10.1007/BF00232485.
- Murata, A., and T. Takizawa (2003), Summertime CO₂ sinks in shelf and slope waters of the western Arctic Ocean, *Cont. Shelf Res.*, 23(8), 753–776, doi:10.1016/S0278-4343(03)00046-3.
- Nightingale, P. D., G. Malin, C. S. Law, A. J. Watson, P. S. Liss, M. I. Liddicoat, J. Boutin, and R. C. Upstill-Goddard (2000), In situ evaluation of air-sea gas exchange parameterizations using novel conservative and volatile tracers, *Global Biogeochem. Cycles*, 14, 373–387, doi:10.1029/1999GB900091.
- Nomura, D., H. Yoshikawa-Inoue, and T. Toyota (2006), The effect of sea-ice growth on air-sea CO₂ flux in a tank experiment, *Tellus, Ser. B*, 58(5), 418–426.
- Omar, A., T. Johannessen, R. G. J. Bellerg, A. Olsen, L. G. Anderson, and C. Kivimäe (2005), Sea-ice and brine formation in Storfjorden: Implications for the Arctic wintertime air-sea CO₂ flux, in *The Nordic Seas: An Integrated Perspective*, *Geophys. Monogr. Ser.*, vol. 158, edited by H. Drange et al., pp. 177–189, AGU, Washington, D. C.
- Omstedt, A. (1985), On supercooling and ice formation in turbulent seawater, *J. Glaciol.*, 31, 263–271.
- Ono, K., A. Miyata, and T. Yamada (2008), Apparent downward CO₂ flux observed with open-path eddy covariance over a non-vegetated surface, *Theor. Appl. Climatol.*, 92(3), 195–208, doi:10.1007/s00704-007-0323-3.
- Prytherch, J., M. J. Yelland, R. W. Pascal, B. I. Moat, I. Skjelvan, and C. C. Neill (2010), Direct measurements of the CO₂ flux over the ocean: Development of a novel method, *Geophys. Res. Lett.*, 37(3), L03607, doi:10.1029/2009GL041482.
- Rysgaard, S., R. N. Glud, M. K. Sejr, J. Bendtsen, and P. B. Christensen (2007), Inorganic carbon transport during sea ice growth and decay: A carbon pump in polar seas, *J. Geophys. Res.*, 112, C03016, doi:10.1029/2006JC003572.
- Rysgaard, S., J. Bendtsen, L. T. Pedersen, H. Ramløv, and R. N. Glud (2009), Increased CO₂ uptake due to sea ice growth and decay in the Nordic Seas, *J. Geophys. Res.*, 114, C09011, doi:10.1029/2008JC005088.
- Shadwick, E., et al. (2011), Seasonal variability of the inorganic carbon system in the Amundsen Gulf region of the southeastern Beaufort Sea, *Limnol. Oceanogr.*, 56(1), 303–322, doi:10.4319/lo.2011.56.1.0303.
- Skogseth, R., F. Nilsen, and L. H. Smedsrud (2009), Supercooled water in an Arctic polynya: observations and modeling, *J. Glaciol.*, 55(189), 43–52.
- Stroeve, J., M. M. Holland, W. Meier, T. Scambos, and M. Serreze (2007), Arctic sea ice decline: Faster than forecast, *Geophys. Res. Lett.*, 34, L09501, doi:10.1029/2007GL029703.
- Sweeney, C., E. Gloor, A. R. Jacobson, R. M. Key, G. McKinley, J. L. Sarmiento, and R. Wanninkhof (2007), Constraining global air-sea gas exchange for CO₂ with recent bomb ¹⁴C measurements, *Global Biogeochem. Cycles*, 21, GB2015, doi:10.1029/2006GB002784.
- Takagaki, N., and S. Komori (2007), Effects of rainfall on mass transfer across the air-water interface, *J. Geophys. Res.*, 112(C6), C06006, doi:10.1029/2006JC003752.
- Takahashi, T., J. Olafsson, J. G. Goddard, D. W. Chipman, and S. C. Sutherland (1993), Seasonal variation of CO₂ and nutrients in the high-latitude surface oceans: A comparative study, *Global Biogeochem. Cycles*, 7(4), 843–878, doi:10.1029/93GB02263.
- Takahashi, T., et al. (2009), Climatological mean and decadal change in surface ocean pCO₂ and net sea-air CO₂ flux over the global oceans, *Deep Sea Res., Part II*, 56(8–10), 554–577, doi:10.1016/j.dsr2.2008.12.009.
- Tsang, G., and T. O. Hanley (1985), Frazil formation in water of different salinities and supercoolings, *J. Glaciol.*, 31(108), 74–85.
- Ushio, S., and M. Wakatsuchi (1993), A laboratory study on supercooling and frazil ice production processes in winter coastal polynyas, *J. Geophys. Res.*, 98(C11), 20,321–20,328.
- Wadhams, P. (2000), *Ice in the Ocean*, Gordon and Breach, New York.
- Wanninkhof, R. (1992), Relationship between wind speed and gas exchange over the ocean, *J. Geophys. Res.*, 97(C5), 7373–7382.
- Wanninkhof, R., and W. R. McGillis (1999), A cubic relationship between gas exchange and wind speed over the ocean, *Geophys. Res. Lett.*, 26, 7373–7381, doi:10.1029/1999GL900363.
- Wanninkhof, R., W. E. Asher, D. T. Ho, C. Sweeney, and W. R. McGillis (2009), Advances in quantifying air-sea gas exchange and environmental forcing, *Annu. Rev. Mar. Sci.*, 1, 213–244.
- Webb, E. K., G. I. Pearman, and R. Leuning (1980), Correction of flux measurements for density effects due to heat and water vapour transfer, *Q. J. R. Meteorol. Soc.*, 106(447), 85–100, doi:10.1002/qj.49710644707.
- Wolf, D. K. (1997), Bubbles and their role in gas exchange, in *The Sea Surface and Global Change*, edited by P. S. Liss and R. A. Duce, pp. 173–207, Cambridge University Press, Cambridge, U. K.
- Wolf, D. K. (2005), Parametrization of gas transfer velocities and sea-state-dependent wave breaking, *Tellus, Ser. B*, 57(2), 87–94, doi:10.1111/j.1600-0889.2005.00139.x.
- Wolf, D. K., et al. (2007), Modelling of bubble-mediated gas transfer: Fundamental principles and a laboratory test, *J. Mar. Syst.*, 66(1–4), 71–91, doi:10.1016/j.jmarsys.2006.02.011.
- Yager, P. L., D. W. R. Wallace, K. M. Johnson, W. O. Smith Jr., P. J. Minnett, and J. W. Deming (1995), The Northeast Water Polynya as an atmospheric CO₂ sink: A seasonal rectification hypothesis, *J. Geophys. Res.*, 100(C3), 4389–4398, doi:10.1029/94JC01962.
- Zappa, C. J., W. E. Asher, A. T. Jessup, J. Klinke, and S. R. Long (2004), Microbreaking and the enhancement of air-water transfer velocity, *J. Geophys. Res.*, 109, C08S16, doi:10.1029/2003JC001897.
- Zappa, C. J., W. R. McGillis, P. A. Raymond, J. B. Edson, E. J. Hints, H. J. Zemmeling, J. W. H. Dacey, and D. T. Ho (2007), Environmental turbulent mixing controls on air-water gas exchange in marine and aquatic systems, *Geophys. Res. Lett.*, 34, L10601, doi:10.1029/2006GL028790.
- Zappa, C. J., D. T. Ho, W. R. McGillis, M. L. Banner, J. W. H. Dacey, L. F. Bliven, B. Ma, and J. Nystuen (2009), Rain-induced turbulence and air-sea gas transfer, *J. Geophys. Res.*, 114, C07009, doi:10.1029/2008JC005008.

W. M. Drennan, Division of Applied Marine Physics, Rosenstiel School of Marine and Atmospheric Science, University of Miami, Miami, FL 33149, USA.

B. G. T. Else, R. J. Galley, and T. N. Papakyriakou, Centre for Earth Observation Science, Department of Environment and Geography, University of Manitoba, 467 Wallace Bldg., 125 Dysart Rd., Winnipeg, MB R3T 2N2, Canada. (b_else@umanitoba.ca)

L. A. Miller, Centre for Ocean Climate Chemistry, Institute of Ocean Sciences, Fisheries and Oceans Canada, PO Box 6000, Sidney, BC V8L 4B2, Canada.

H. Thomas, Department of Oceanography, Dalhousie University, 1355 Oxford St., Halifax, NS B3H 4J1, Canada.